

## Friction heat production and atom diffusion behaviors during Mg–Ti rotating friction welding process

LI Rui-di<sup>1,2</sup>, LI Jing-long<sup>1,2</sup>, XIONG Jiang-tao<sup>1,2</sup>, ZHANG Fu-sheng<sup>1,2</sup>, ZHAO Ke<sup>1,2</sup>, JI Cheng-zhong<sup>1,2</sup>

1. State Key Laboratory of Solidification Processing, Northwestern Polytechnical University, Xi'an 710072, China;
2. Shaanxi Key Laboratory of Friction Welding Technologies, Northwestern Polytechnical University, Xi'an 710072, China

Received 1 November 2011; accepted 27 August 2012

**Abstract:** An innovative physical simulation apparatus, including high speed camera, red thermal imaging system, and mechanical quantity sensor, was used to investigate the friction heat generation and atom diffusion behavior during Mg–Ti friction welding process. The results show that the friction coefficient mainly experiences two steady stages. The first steady stage corresponds to the Coulomb friction with material abrasion. The second steady stage corresponds to the stick friction with fully plastic flow. Moreover, the increasing rates of axial displacement, temperature and friction coefficient are obviously enhanced with the increase of rotation speed and axial pressure. It can also be found that there exists rapid diffusion phenomenon in the Mg–Ti friction welding system. The large deformation activated diffusion coefficient is about  $10^5$  higher than that activated by thermal.

**Key words:** Mg–Ti; friction welding; rotating friction welding; heat generation; atom diffusion; friction coefficient; Coulomb friction; stick friction

### 1 Introduction

Friction welding, as a typical solid state joining technology, enables the high quality welding between two parts with similar or dissimilar materials, and has aroused growing interest in many practical engineering fields. During the friction welding process, the contact interfaces of two components are compelled to rub against each other, leading to the heat production at the rub interface. Then the contact interfaces were heated and softened, accompanied with material flow, dynamic recrystallization and atom diffusion [1,2]. Consequently, a detailed understanding of heat generation and atom diffusion during the friction welding process is significantly important for controlling and improving the welding process.

In the aspect of heat generation, the coefficient of friction has a significant influence on the heat generation and accordingly temperature field [3]. The thermal models that describe a precise temperature of friction welding process need accurate frictional data, such as the friction coefficient. In the beginning of the research of

rotating friction welding or friction stir welding, many researchers adopted a constant friction coefficient to quantitatively characterize the heat generation and temperature [4–6]. But the friction during friction welding process experiences low temperature to high temperature [7], during which the material properties are changed from elastic state to viscoplastic state, resulting in a variant friction coefficient. Since then, a rigid viscoplastic materials model was proposed, in which the torsional friction was used to characterize the heat generation of friction welding [4,8]. They pointed out that the friction experienced Coulomb friction in a low-temperature range, and a high-temperature range in which the shear yield stress was equal to friction stress. Although the simulation study based on the sliding-sticking model was found to fit for the experiment result [9], the model failed to establish a rule differentiating the low and high temperature ranges. In the other aspect of atom diffusion of friction welding, the particularity is that the diffusion is not only activated by thermal, but also enhanced by large stress, due to the strongly thermal and stress coupled nature of friction welding. Although previous literatures reported the stress

**Foundation item:** Projects (51101126, 51071123) supported by the National Natural Science Foundation of China; Projects (20110491684, 2012T50817) supported by the China Postdoctoral Science Foundation; Project (20110942K) supported by the Open Fund of State Key Laboratory of Powder Metallurgy of Central South University, China

**Corresponding author:** LI Rui-di; Tel: +86-29-88491426; Fax: +86-29-88491426; E-mail: [liruidi@126.com](mailto:liruidi@126.com)  
DOI: 10.1016/S1003-6326(11)61515-X

hence diffusion phenomenon in friction welding process [10,11], the detailed influencing factors were still not clear. Above all, the previous researches have not addressed heat generation and atom diffusion accurately and convincingly, thus a further investigation is, thereby, necessary.

In this work, an innovative physical simulation apparatus of friction welding, including high speed camera, red thermal imaging system, and mechanical quantity sensor, was set up to investigate the friction heat generation and atom diffusion. The axial displacement, friction temperature, mechanical parameters, friction coefficient, microstructure and atom diffusion characteristics under different rotate speeds and axial pressures were detected.

## 2 Experimental

Commercially pure titanium and magnesium alloy (ZK61) were used, and the dimensions are schematically shown in Fig. 1. Before the friction welding, the Mg alloy rod was rotated around its axis while the Ti rod was irrotational. When the rotation speed reached the pre-established parameter, the Ti rod moved along the axis then contacted with the Mg alloy rod under the action of hydraulic pressure, thus the friction process began. After the end of the friction, no upsetting procedure was applied due to the fact that it has no use for the present study. The friction welding parameters were: rotation speed 800–1600 r/min, axial pressure 6–10 kN. In the meanwhile, the axial displacement and the welding image were observed by a high-speed camera (Vision Research Inc, Phantom v 310) with a frame rate of 500 fps. The temperature field of the welding process was collected by a red thermal imaging system (InfraTec, VarioCAM@hr head-HS) with the frame rate of 60 fps. The infrared emitting ability was assumed as 1. The torque and normal pressure applied on the friction rods were obtained by a mechanical quantity sensor with frequency of 1000 Hz. At last, the welded sample for metallographic examination was cut perpendicular to the welding interface. Then the samples for metallographic analysis were produced by standard means. The microstructures were analyzed by a scanning electron microscope (SEM). The chemical composition was obtained by energy dispersive X-ray (EDX) spectrometer analysis.

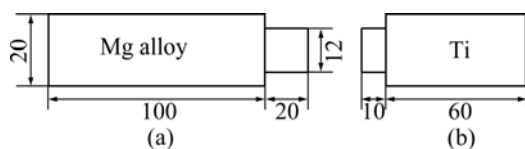


**Fig. 1** Schematic diagram showing dimensions of Mg alloy (a) and Ti bars (b)

## 3 Results

The axial displacements of Ti rod as a function of time under different rotation speeds were collected by a high speed camera system, as shown in Fig. 2. The axial pressure of 7.5 kN was fixed as constant. It can be found that the friction welding process experienced two processes at any rotation speed. In the first friction process, there was no visible axial shortening because it was the beginning stage that the Ti rod contacted the rotating Mg alloy rod while the friction heat was inadequate to soften the metal at the friction interface. In the second friction process, there was clear axial shortening due to the adequate friction heat and accordingly high temperature which could soften the metal at friction interface and form the flashing. By comparing the different rotation speeds, it can be found that the time used for the appearance of axial shortening was lessened with the increase of rotation speed. Moreover, with the increase of rotation speed, the axial shortening quantity increased at the same friction time. In other words, the axial shortening speed was increased with increasing the rotation speed. It was because that increasing the rotation speed could enhance the input power of friction welding, leading to the shorter time for the heat generation, softening, plastic deformation and axial displacement. Figure 3 shows the axial displacement of Ti rod as a function of time under different axial pressures. The rotation speed of 1200 r/min was fixed as constant. This indicated that the time for appearance of axial displacement was lessened with increasing the axial pressure. Furthermore, the increase of the axial pressure can enable a high axial displacement at the same friction time. In other words, the axial shortening occurred more quickly as the high axial pressure was applied. This was because that during the friction process, the input power of friction heat was

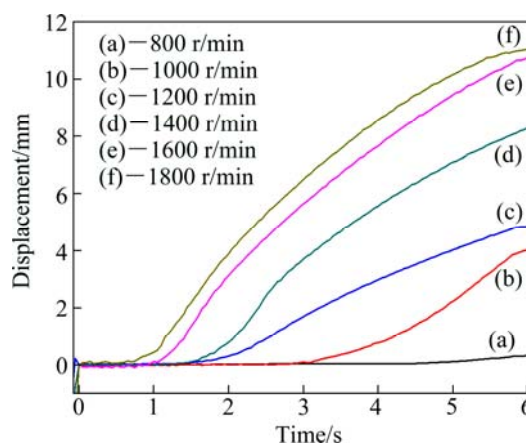


**Fig. 2** Axial displacement of Ti rod as function of time under different rotation speeds

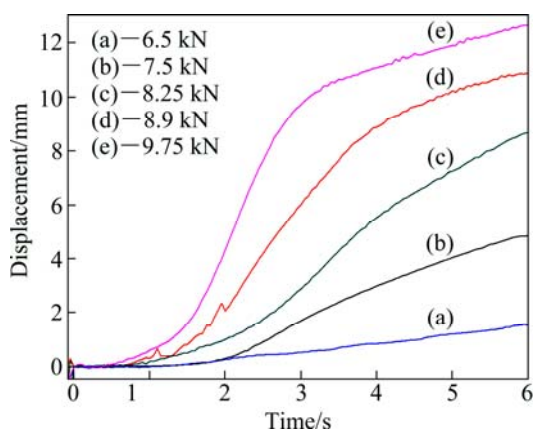


**Fig. 3** Axial displacement of Ti rod as function of time under different axial pressures

governed by the friction work. When a high axial pressure was applied, the input power was enhanced, leading to quick heat generation, metal softening and resultant axial displacement.

The temperature of flash external as a function of time under different rotation speeds were measured by red thermal imaging system, as indicated in Fig. 4. It revealed that the temperature variation contained two stages. The temperature firstly experienced a rising stage, and then reached a steady state no matter at any rotation speed. More interestingly, it can be found that the temperature was contiguous at any rotation speed when the friction reached the steady stage. By comparing the temperature variant curves at different rotation speeds, it can be found that the rotation speed had a notable influence on the temperature rising curve. At a relatively lower rotation speed from 800 to 1400 r/min, the temperature and the heating rate were enhanced with increasing the rotation speed. However, when a higher rotation speed from 1400 to 1800 r/min was applied, the heating rate showed a little change under different rotation speeds. In addition, it should be noted that

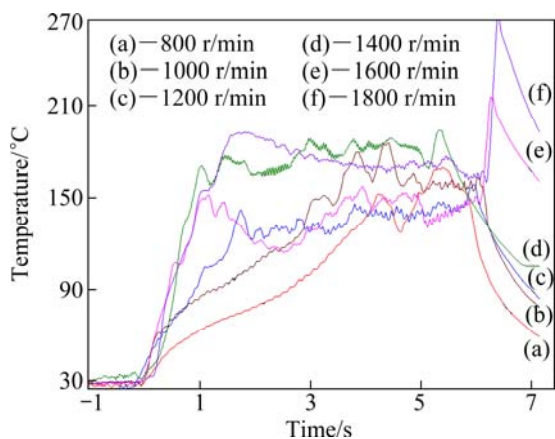


**Fig. 4** Temperature of flash external as function of time under different rotation speeds

during the friction welding process, the Ti rod had no deformation and inserted into the Mg alloy rod, so the temperature obtained by infrared video camera was the flash external temperature, which was below the friction interface temperature. However, the variation trend under different welding parameters can be obtained. Figure 5 shows the temperature as a function of time under different axial pressures. Generally, the heating process also obeyed the rising stage and the steady stage. Moreover, it can be found that a higher axial pressure could enable the relative temperature, although the axial pressure had a modest effect on the temperature.

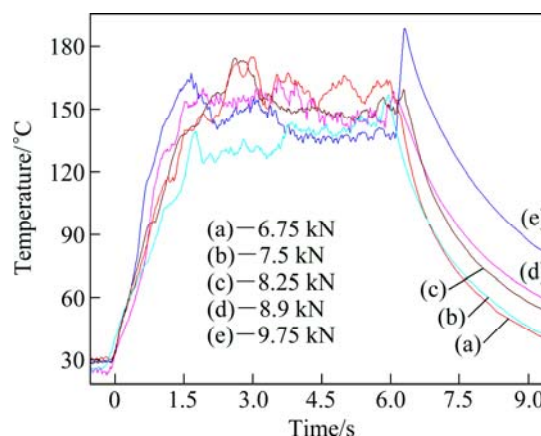


**Fig. 5** Temperature of flash external as function of time under different axial pressures

The friction coefficients under different rotation speeds were measured by mechanical quantity sensor, as clearly indicated in Fig. 6. It was obvious from Fig. 6 that the friction coefficient experienced two rising stages, two steady stages, two overshooting and fallback stages at any rotation speeds. Concretely speaking, the friction coefficient firstly experienced a rapid rising stage from 0 to about 0.15, and instantaneously an overshooting and fallback phenomenon appeared, and then the friction coefficient reached a steady stage of about 0.1. Afterward, the friction coefficient experienced the second rising stage from 0.1 to 0.45 coupled with the second overshooting and fallback phenomenon, and then reached the second steady stage of about 0.35. Although all the friction coefficients were present in similar variant stages, the rising rate in the second rising stage was found to vary with the rotation speed. It was clear that a higher rotation speed could yield a more rapid rising rate especially in the second rising stage. Figure 7 presents the effect of axial pressure on the friction coefficient versus time curves. At relatively lower axial pressures (6–7.5 kN), the friction coefficient versus time curves were present in two rising and steady stages. However, when higher axial pressures (8.25–9.75 kN) were applied, the friction coefficient versus time curves presented one

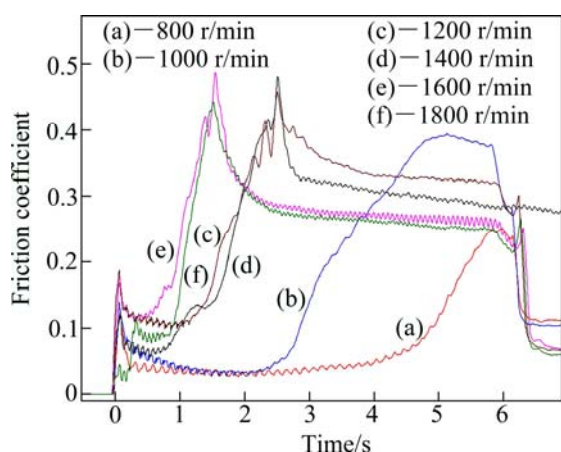


Fig. 6 Friction coefficient as function of time under different rotation speeds

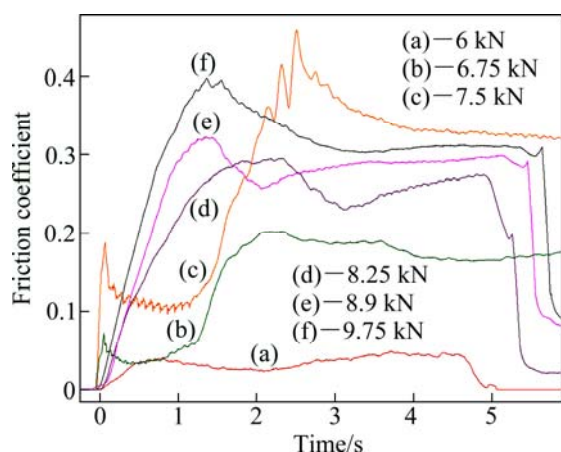


Fig. 7 Friction coefficient as function of time under different axial pressures

rising steady stage only. Overall, it also revealed that a high axial pressure could enable a rapid rising rate.

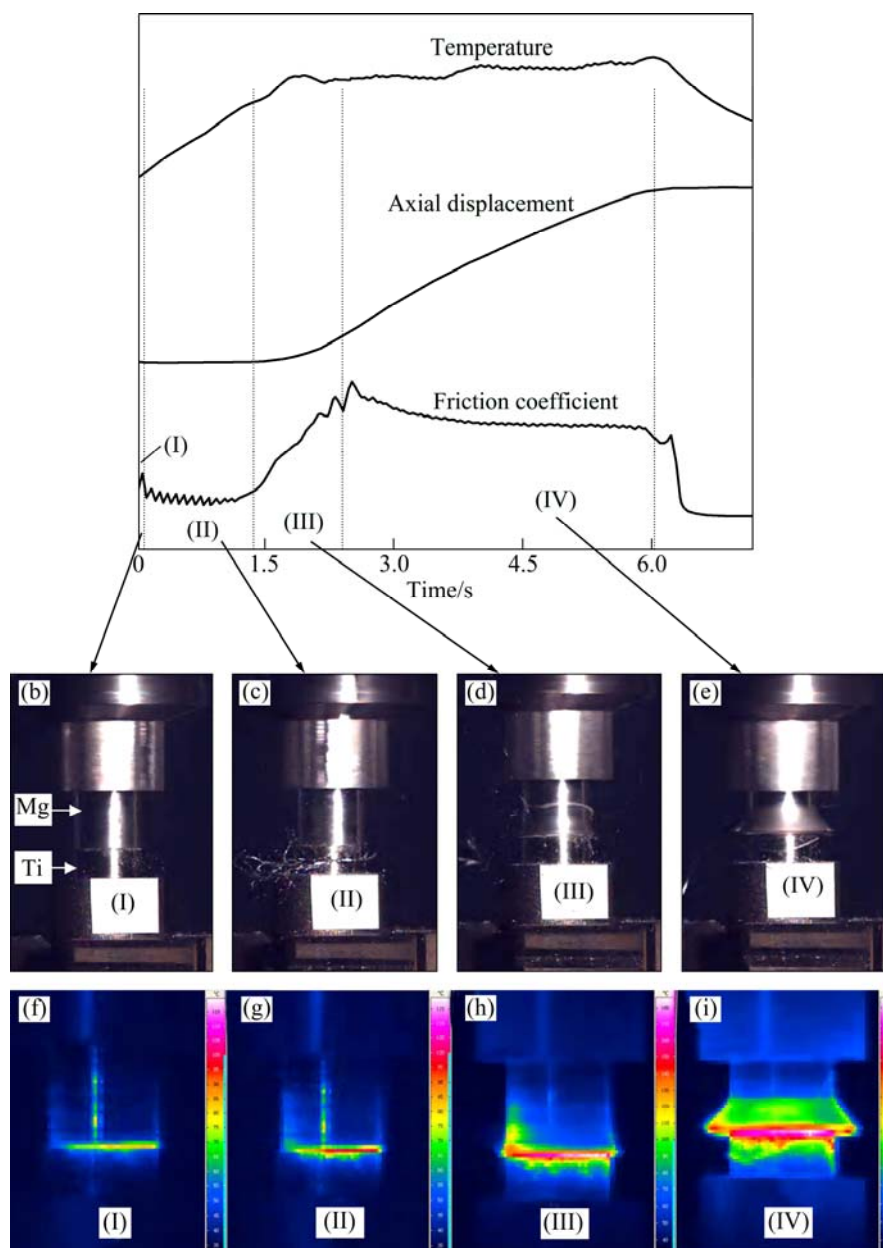
In order to understand the relationship among above parameters, the curves of temperature, axial displacement and friction coefficient versus time are shown in Fig. 8(a). Figures 8(b–e) show the exterior morphologies of friction rods in different friction stages taken by high-speed photography. Figures 8(f–i) present the temperature field of friction rods in different friction stages obtained by red thermal imaging system. In general, one can notice that the variant of various parameters can be divided into four stages. In the first friction stage, there were no axial displacement and friction chip (Fig. 8(b)). In the meantime, the temperature rising of friction interface was also not obvious, coupled with the rapid increase of friction coefficient from 0 to about 1.5. In the second stage, although the friction chips were formed (Fig. 8(c)), the axial displacement was not obvious, but the temperature rising of the friction interface was apparent. At the same

time, the friction coefficient reached a platform. In the third stage, the temperature has been elevated to a maximum value, and the axial displacement tended to occur, accompanied with the gradual increase of friction coefficient. It was obvious that the friction flashing appeared for Mg rod due to the plastic flow (Fig. 8(d)). In the fourth stage, the temperature and friction coefficient reached steady stages while the axial displacement increased continuously. Meanwhile, the plastic deformation of Mg rod was obvious (Fig. 8(e)).

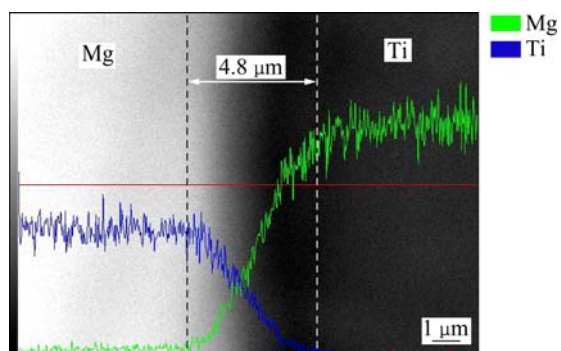
Figure 9 shows the SEM image of backscattered electron (BSE) mode and the EDX result of Mg–Ti friction welding interface at a rotation speed of 1000 r/min. The EDX result indicated that there existed inter diffusion zone at the Mg–Ti interface with the depth of about 4.8  $\mu\text{m}$ . Similarly, the diffusion depths under different rotation speeds were measured according to this method, as shown in Table 1. It revealed that the diffusion depth was increased. According to the parabolic protocols, the diffusion coefficient was calculated by  $D=x^2/t$ , where  $x$  is the diffusion depth and  $t$  is the diffusion time. The diffusion coefficients are listed in Table 1. In our previous work, the vacuum diffusion welding of Mg and Ti was conducted, and the relevant diffusion coefficient was  $2 \times 10^{-17} - 6 \times 10^{-17} \text{ m}^2/\text{s}$  [12]. Therefore, it was obvious that during friction welding process the plastic deformation activated diffusion coefficient is  $10^5$  higher than thermal activated diffusion coefficient. It should be noted that the diffusion coefficient has correlations with temperature, crystal structure, and crystal defects. In this work, we consider the differences between friction welding and diffusion welding as follows. The atom diffusion during diffusion welding is mainly promoted by temperature. However, the atom diffusion during friction welding is not only promoted by temperature, but also by severe deformation. The temperatures of diffusion welding and friction welding are similar, so we can infer that the enhanced diffusion coefficient of friction welding is caused by stress and severe deformation.

Table 1 Diffusion conditions at different rotation speeds

Rotation speed/(r·min <sup>-1</sup> )	Diffusion depth/ $\mu\text{m}$	Diffusion coefficient/( $10^{-12}\text{m}^2\cdot\text{s}^{-1}$ )
1000	4.8	3.84
1200	4.8	3.84
1400	4.7	3.68
1600	5.1	4.34
1800	6.4	6.83



**Fig. 8** Variation of axial displacement, temperature and coefficient versus time at rotation speed of 1200 r/min and axial pressure of 7.5 kN: (a) Relationship among parameters; (b)–(e) Exterior morphologies of friction rods at different stages; (f)–(i) Temperature field of friction rods at different stages



**Fig. 9** BSE image and EDX result of Mg–Ti friction interface at 1000 r/min

## 4 Discussion

Above results indicated that the friction coefficients exhibited two steady stages in any friction conditions, which can be understood as follows. The two different friction coefficient steadies corresponded to totally different friction mechanisms. In the first friction steady stage, the friction mechanism is sliding and the friction type is Coulomb friction, because the corresponding temperature is low (Fig. 8(g)) and there is no occurrence of plastic flow (Fig. 8(c)). Although the contact interfaces seem smooth in macroscopic level, the friction

interface is not smooth but there exist many irregularities in microscopic level. The actual contacts are made between the asperities of the two interfaces and the real contact area is small than the apparent contact area. Moreover, in this steady stage the friction stress is lower than the shear yield stress. However, with the proceeding of heat generation, the temperature of friction interface is enhanced gradually (Fig. 8(i)), thereby inducing a full plastic flow (Fig. 8(e)) at the friction interface, whose friction mechanism is sticking [4]. In this steady stage, the real contact area is close to the apparent area and the friction stress is equal or higher than the shear yield stress of material and independent of axial pressure. Therefore, it is reasonable to conclude that the first friction steady stage is sliding and the second friction steady stage is sticking.

During friction process, the heat generation is derived from friction and plastic deformation. Thus the heat power can be expressed as [4]

$$q=(1-x)f\upsilon+x\eta\tau v \quad (1)$$

where  $x$  expresses the extent of sticking mechanism;  $f$  the friction stress;  $v$  is the friction speed;  $\eta$  is the thermal power conversion efficiency; and  $\tau$  is the shear yield stress. When the friction is in the first steady stage, the heat is generated by Coulombic friction and the  $x$  is 0. When the friction enters the second steady stage, the interface is filled with high temperature plastic metal which induces the heat generation and the  $x$  is 1. Therefore, when the friction is in the overmixing stage of the two steady stages, the two heat generation mechanisms coexist. This indicates that with the increase of friction speed and axial pressure the friction power increases, inducing a higher thermal flow density and accordingly rising rates of temperature, axial displacement and friction coefficient. Thus a high friction speed and axial pressure could enable the rapid increase of axial displacement, temperature rising and increase of friction coefficient.

During the large deformation process, the rapid atom diffusion phenomenon has been detected in many other material processing technologies, such as the mechanical alloying [13], ultrasonic welding [14], and friction stir processing [15]. This is because that many vacancies tend to be occurred during the large deformation process. The vacancies could induce the atom diffusion significantly during friction welding, due to large deformation at the action of the highly thermal and stress coupled effect. However, the detailed mechanisms of deformation enhanced diffusion are still not clear and will be an important research direction in the further.

## 5 Conclusions

1) The friction welding of Mg–Ti experiences two

steady stages and two transitional stages. The first steady stage corresponds to the Coulomb friction with materials abrasion. The second steady stage corresponds to the stick friction with fully plastic flow.

2) With the increase of rotation speed or axial pressure, the friction power is enhanced, leading to the rapid transformation to the steady of the axial displacement, temperature and friction coefficient during friction welding process.

3) During rotation friction welding process, the atom diffusion is enhanced significantly by a large plastic deformation at the Mg–Ti interface. The diffusion coefficient activated by deformation is  $10^5$  higher than that activated by thermal.

## References

- [1] PEW J W, NELSON T W, SORENSEN C D. Torque based weld power model for friction stir welding [J]. *Science and Technology of Welding and Joining*, 2007, 12(4): 341–347.
- [2] UDAY M B, FAUZI M N A, ZUHAILAWATI H, ISMAIL A B. Advances in friction welding process: a review [J]. *Science and Technology of Welding and Joining*, 2010, 15(7): 534–558.
- [3] SCHNEIDER J, BESHEARS R, NUNES A C. Interfacial sticking and slipping in the friction stir welding process [J]. *Materials Science and Engineering A*, 2006, 435: 297–304.
- [4] MAALEKIAN M, KOZESCHNIK E, BRANTNER H P, CERIAK H. Comparative analysis of heat generation in friction welding of steel bars [J]. *Acta Materialia*, 2008, 56(12): 2843–2855.
- [5] MISHRA R S, MA Z Y. Friction stir welding and processing [J]. *Materials Science and Engineering R*, 2005, 50(1–2): 1–78.
- [6] KOVACEVIC R, CHEN C M. Finite element modeling of friction stir welding — Thermal and thermomechanical analysis [J]. *International Journal of Machine Tools & Manufacture*, 2003, 43(13): 1319–1326.
- [7] MAALEKIAN M. Thermal modeling of friction welding [J]. *Isij International*, 2008, 48(10): 1429–1433.
- [8] ZHANG Q Z, ZHANG L W, LIU W W, ZHANG X G, ZHU W H, QU S. 3D rigid viscoplastic FE modelling of continuous drive friction welding process [J]. *Science and Technology of Welding and Joining*, 2006, 11(6): 737–743.
- [9] NANDAN R, ROY G G, LIENERT T J, DEBROY T. Three-dimensional heat and material flow during friction stir welding of mild steel [J]. *Acta Materialia*, 2007, 55(3): 883–895.
- [10] JIN H W, AYER R, MUELLER R R, LING S, FORD S. Interface structure in a Fe–Ni friction stir welded joint [J]. *Scripta Materialia*, 2005, 53(12): 1383–1387.
- [11] XIONG J T, ZHANG F S, LI J L, QIAN J W, HUANG W D. In-Situ synthesized Al(3)Ni–Al composites by friction stir processing [J]. *Rare Metal Materials and Engineering*, 2010, 39(1): 139–143.
- [12] LI Xue-fi. Atomic superdiffusion in Mg–Ti system under severe deformation of friction stir processing [D]. Xi'an: Northwest Polytechnical University, 2010: 21–31. (in Chinese)
- [13] SAUVAGE X, WESTSCHER F, PAREIGE P. Mechanical alloying of Cu and Fe induced by severe plastic deformation of a Cu–Fe composite [J]. *Acta Materialia*, 2005, 53(7): 2127–2135.
- [14] LI M Y, JI H J, WANG C Q, BANG H S, BANG H S. Interdiffusion of Al–Ni system enhanced by ultrasonic vibration at ambient temperature [J]. *Scripta Materialia*, 2006, 45(1–4): 61–65.
- [15] XIONG J T, ZHANG F S, LI J L, QIAN J W, HUANG W D. In-situ synthesized Al3Ni–Al composites by friction stir processing [J]. *Rare Metal Materials and Engineering*, 2010, 39(1): 139–143.

# Mg-Ti 旋转摩擦焊过程的摩擦产热及原子扩散行为

李瑞迪<sup>1,2</sup>, 李京龙<sup>1,2</sup>, 熊江涛<sup>1,2</sup>, 张赋升<sup>1,2</sup>, 赵科<sup>1,2</sup>, 籍成宗<sup>1,2</sup>

1. 西北工业大学 凝固技术国家重点实验室, 西安 710072;

2. 西北工业大学 陕西省摩擦焊接重点实验室, 西安 710072

**摘要:** 利用新型物理模拟装置进行 Mg-Ti 旋转摩擦焊过程产热机理及原子扩散行为的研究, 该装置包含高速摄像、红外热成像及力学传感器系统。结果表明, 摩擦焊过程中, 摩擦因数经历两个稳态阶段的变化。第一个稳态阶段为库伦摩擦, 以磨蚀为主要形式; 第二个稳态阶段为粘着摩擦, 以塑性流动为主要形式。另外, 随着旋转转速及轴向压力的提高, 轴向位移、摩擦温度及摩擦系数的增加率也随之明显提高。Mg-Ti 摩擦焊过程存在原子的快速扩散现象, 该过程中由摩擦大变形激活的扩散系数大约是热激活扩散系数的  $10^5$  倍。

**关键词:** Mg-Ti; 摩擦焊; 旋转摩擦焊; 产热; 原子扩散; 摩擦因数; 库仑摩擦; 粘着摩擦

(Edited by LI Xiang-qun)